HiSST: 2nd International Conference on
High-Speed Vehicle Science & Technology
11–15 September 2022, Bruges, Belgium

Multi-Objective Design Optimization of Scramjet Intakes via Evolutionary Algorithms Assisted by Multi-Dimensional Predictive Modeling Based on Deep Learning

Chihiro Fujio[1], *Hideaki Ogawa*[2]

Abstract

Design of scramjet intakes requires sophisticated methodologies to achieve desirable compression reducing total pressure loss and drag simultaneously, and multi-objective design optimization (MDO) using evolutionary algorithms (EA) is one of the most promising approaches. In addition, the dataset obtained from computational fluid dynamics (CFD) simulations in the MDO process can serve expected as a rich mine of physics-based information. However, the substantial computational cost of a large number of CFD evaluations represents an obstacle to high-fidelity design search. The present study proposes an evolutionary algorithm which employs a multi-dimensional flow prediction model via deep learning for objective/constraint function evaluations to replace CFD simulation by predicting flowfields inside scramjet intakes. The proposed EA-based MDO framework is applied to an optimization study of axisymmetric 3-ramp intakes and the performance and utility are discussed. This EA approach using multi-dimensional predictive modeling is applicable for various optimization problems which require reduction of the computational cost of function evaluations.

Keywords: *Hypersonic airbreathing propulsion, Scramjet intake, Multi-objective design optimization, Evolutionary algorithm, Deep learning*

1. Introduction

Scramjet (supersonic combustion ramjet) engines are an air-breathing technology that operates under hypersonic conditions and can be used for high-speed point-to-point (P2P) transportation as well as atmospheric ascent flights in space transportation. Scramjet engines are expected to be one of the key technologies to realize low-cost and flexible space transportation due to efficient engine operation and maneuvability. Scramjet research and technology developments have been continued since the 1940s and advanced to the level of flight tests [1, 2]. Among the main components of a scramjet engine (*e.g.*, an air intake, fuel injectors, a combustor, and a nozzle), the air intake, which lies most upstream in the scramjet flow path, plays a key role in achieving successful operation of the scramjet engines by determining the characteristics of internal flowfields. The performance of scramjet intakes is examined with respect to various aspects such as the capability of compression, efficiency, and robustness, and multi-objective design optimization (MDO) is recognized as an effective design technique due to the capability of exploring the design space for optimum solutions by taking multiple design criteria into account simultaneously.

Evolutionary algorithms (EAs) are one of the most effective approaches for multi-objective design optimization due to their ability to find a wide variety of optimal solutions without user-defined fixed-ups for multi-objective optimization problems [3]. The algorithms enable identification of optimum solutions while maintaining the diversity of solutions, and thus the resultant set of optimum solutions serves as an archive of various superior designs. Further, the numerous solution evaluations accordingly yield a dataset that may offer useful insights via data mining. Preceding studies include the design optimization

[1]*Department of Aeronautics and Astronautics, Kyushu University, 744 Motooka, Nishi-ku, Fukuoka 819-0395, Japan, fujio.chihiro.354@s.kyushu-u.ac.jp*
[2]*Department of Aeronautics and Astronautics, Kyushu University, 744 Motooka, Nishi-ku, Fukuoka 819-0395, Japan, hideaki.ogawa@aero.kyushu-u.ac.jp*

and data mining for airfoil shapes [4], wings of a flyback booster [5], and scramjet intakes [6]. While these studies have demonstrated that EAs can produce not only excellent design but also important knowledge for the design strategies, considerable computational cost for function evaluations inherently hampers EAs from revealing their potential. Reduction of computational costs for function evaluations has been a subject of interest and surrogate models are often employed to replace the true function evaluations which require large computational costs [7]. A surrogate model typically predicts an objective/constraint function value for a given set of decision variable values as the inputs. Since the relation between an objective/constraint function and decision variables is represented by a function, the computational cost can be reduced significantly compared to that of true function evaluations which involve computationally expensive simulations. However, the reduction of computational costs may sacrifice the fidelity of design search and affect an important role of EAs in providing key insights into the design problem since surrogate models do not represent physics-based behavior. Such drawback of surrogate modeling have motivated the development of predictive modeling that can provide the same amount of multi-dimensional physical information as the numerical simulation which is employed in true function evaluations.

The development of multi-dimensional predictive modeling which allows for prediction of flowfields (hence multi-dimensional output) rather than scalar values has been accelerated by recent advances in machine learning and computer technologies. Many researchers conducted studies on prediction of various flowfields by using various machine learning techniques in recent years [8]. The prediction methodologies can be classified into reduced-order-modeling-based (ROM-based) approaches and direct predictions. The former couples ROM for feature extraction and regression techniques for prediction. Proper orthogonal decomposition (POD) and dynamic mode decomposition (DMD) are often employed for the order reduction [9, 10]. The ROM-based approaches have advantages in the computational cost but the nature of order reduction inherently affects the prediction accuracy. On the other hand, direct prediction does not involve order reduction and thus tends to enable more accurate prediction than those using ROM despite tendency of larger computational cost for modeling. The direct prediction models via deep learning have been reported for airfoils and scramjet intakes in previous studies [11, 12]. While ROM-based approaches typically predict just one flow property, deep-learning models can predict multiple properties by one model. Deep-learning direct prediction modeling is employed in the present study based on the preceding study [12] since the performance of scramjet intakes is assessed by using multiple flow properties.

The present study aims to develop a low-cost and high-fidelity design methodology for scramjet intakes which provides not only a set of optimal designs but also physical insights into the design. An evolutionary algorithm which employs multi-dimensional predictive modeling for function evaluation (multi-dimensional prediction assisted evolutionary algorithms, MDPAEA) is proposed. Deep learning techniques realize multi-dimensional predictictive modeling to predict flowfields inside scramjet intakes instead of scalar values. The MDPAEA framework is validated by using 3 test problems and an optimization study of axisymmetric 3-ramp intake design is conducted by using MDPAEA. The ability and performance of MDPAEA are examined by scrutinizing the optimization results in terms of computational efficiency, solution search, and model accuracy.

2. Methodologies

2.1. Configuration

The present study considers scramjet intakes for ascending flight in space transportation. The ascent trajectory assumes a constant dynamic pressure at 49.7 kPa in consideration of the limitation of engine structure and supersonic combustion. It assumes typical flow conditions where the scramjet starts the operation, *i.e.*, Mach number M_∞=7.7, static pressure p_∞=1197 Pa, and static temperature T_∞=226.5 K at an altitude of 30 km.

An axisymmetric 3-ramp intake configuration is employed in the present study due to its high efficiency and simple structure[13]. The configuration and parametrization are shown schematically in Fig. 1. θ_1 is the inclination angle of the 1^{st} ramp and $\Delta\theta_2$ and $\Delta\theta_3$ are the increments of wall inclination angle at the 2^{nd} and 3^{rd} ramps. The length of the i^{th} ramp is represented by l_i and the total intake length

is represented by l. The radii at the intake entrance and exit are r_{i} and r_{c}, respectively. The intake entrance radius is fixed at 0.075 m to maintain a constant mass flow rate. Among these 7 parameters except for the intake entrance radius r_{i}, the 6 parameters except for l_1 are used to determine intake geometries, whereas the 1st ramp length l_1 can be calculated by using the other parameters.

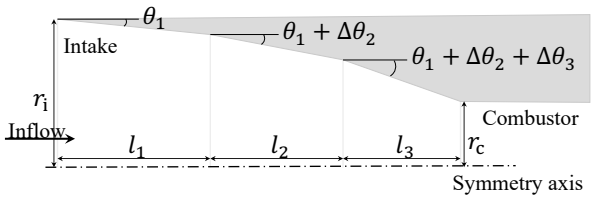

Fig 1. Parameterization of axisymmetric 3-ramp intake

2.2. Design optimization

The fundamental performance criterion of scramjet intakes is the capability of compression, which is assessed based on the compression (static pressure) ratio and/or mean static temperature at the intake exit. Therefore, mean exit temperature $\bar{T}_2$ is employed as a constraint function to impose a minimum requirement for compression. In the present study, mean exit temperature is required to be larger than 850 K, *i.e.*, $\bar{T}_2 \geq 850$ K. High-performance intakes are characterized by high compression efficiency hence low total pressure loss and low drag generation. Compression efficiency loss $1 - \eta_{\mathrm{B}}$ and drag are employed as the objective functions to be minimized. The present optimization problem can thus be described as below:

$$\begin{aligned} \textit{Miminize}: \quad & 1 - \eta_{\mathrm{B}} \\ & \text{Drag [N]} \\ \textit{Subject to}: \quad & \bar{T}_2 > 850 \text{ [K]} \\ & \epsilon_{\mathrm{convergence}} > 0 \end{aligned}$$

where $\epsilon_{\mathrm{convergence}}$ represents the convergence of CFD simulation ($\epsilon_{\mathrm{convergence}}$=1 for converged solutions and $\epsilon_{\mathrm{convergence}}$=-1 for other solutions). Compression efficiency is calculated as follows:

$$\eta_{\mathrm{B}} = \frac{\bar{T}_1}{\bar{T}_2 - \bar{T}_1} \left\{ \left(CR \sqrt{\frac{\bar{T}_{01} - \bar{T}_1}{\bar{T}_{01} + \frac{\Delta Q}{c_p \dot{m}} - \bar{T}_2}} \frac{\bar{T}_2}{\bar{T}_1} \right)^{\frac{\gamma-1}{\gamma}} - 1 \right\} \tag{1}$$

where CR is the contraction ratio, $\bar{T}_0$ is total temperature, ΔQ is the total heat transfer across the intake wall, c_p is specific heat at a constant pressure, γ is specific heat ratio, and $\dot{m}$ is the mass flow rate. The top bar denotes stream-thrust averaged flow properties (*e.g.*, $\bar{T}$ is stream-thrust averaged static temperature). Drag can be calculated as below:

$$\text{Drag} = F_{\mathrm{in}} - \dot{m} \frac{2\left(h_0 + \frac{\Delta Q}{\dot{m}} - \bar{h}_2\right) + R\bar{T}_2}{\sqrt{2\left(h_0 + \frac{\Delta Q}{\dot{m}} - \bar{h}_2\right)}} \tag{2}$$

where F_{in} is the streamwise force acting on the intake entrance, h_0 is total enthalpy, and R is the gas constant of air. These expressions are derived by Fujio and Ogawa [14] for compression efficiency (Eq. (1)) and Ogawa and Boyce [15] for drag (Eq. (2)).

The solutions are defined by 6 decision variables, which are the 6 design parameters introduced in Sec. 2.1. The ranges of the decision variables are summarized in Table 1.

Table 1. Upper and lower limits of design variables

Design variable	Unit	Lower limit	Upper limit
θ_1	deg	3.5	6.5
$\Delta\theta_2$	deg	2.5	5.5
$\Delta\theta_3$	deg	0.5	4.0
l_2	m	0.03	0.07
l_3	m	0.01	0.05
r_c	m	0.02	0.04

2.3. multi-dimensional prediction assisted evolutionary algorithm

A multi-dimensional prediction assisted evolutionary algorithm (MDPAEA) is developed for the multi-objective design optimization (MDO) problems. The optimization chain is displayed schematically in Fig. 2. The algorithm employs deep learning prediction for objective/constraint function evaluations. A predictive model is prepared in advance of the optimization loop and a training dataset is used to select initial population of the evolutionary algorithm. The prediction from the model is employed if the relative prediction error for the objective/constraint functions is less than 5 %. The model is improved via transfer learning every 10 generations. Detailed information on the modeling and prediction approached is provided in Sec. 2.4.

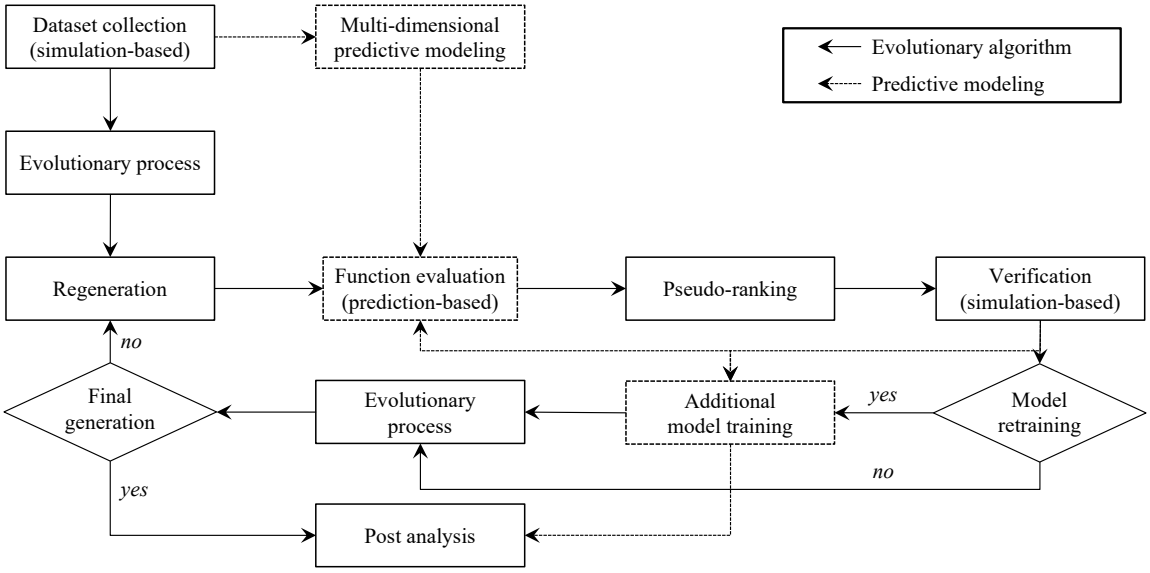

Fig 2. Optimization chain of multi-dimensional prediction assisted evolutionary algorithm

The evolutionary process is based on the non-dominated sorting evolutionary algorithm NSGA-II proposed by Deb *et al.* [16]. The process consists of 4 steps, *i.e.*, objective/constraint function evaluation, ranking, selection, and regeneration. All individuals in the i^{th} generation are evaluated by using model prediction at first, and then are ranked in conjunction with the individuals in the $(i-1)^{\text{th}}$ generation based on objective/constraint functions that are calculated using the model prediction ("pseudo-ranking" in Fig. 2). Among the individuals, the first-ranked individuals, namely non-dominated individuals at the generation are verified via true function evaluation (CFD in the present study). The data of true function evaluations are stored in an archive which is used for model updates. After the verification of the provisional non-dominated individuals, ranking is performed again to determine the actual ranks of the individuals. Then, the selection is conducted based on dominance and crowding distance. The lowest

rank is assigned to infeasible individuals, which are sorted based on constraint violations. Tournaments are then conducted among surviving individuals to select parent individuals for regeneration. In the regeneration process, crossover and mutation are conducted via simulated binary crossover (SBX) and polynomial mutation with distribution indices for crossover and mutation of 10 and 20, respectively. These evolutionary processes are iterated until the final generation.

2.4. Multi-dimensional predictive modeling via deep learning

2.4.1. Prediction & training

Multilayer perceptron (MLP) is employed to predict flowfields inside scramjet intakes based on the 6 design parameters defined in Table 1. The model is generated using an open-source Python library, Tensorflow [17]. The model predicts static pressure, static temperature, and axial and radial velocity components at a given location inside the intake. Thus, the model employs 8 parameters (6 design variables and 2 coordinate variables (x, r)) as the inputs and has 4 output parameters as seen in Fig. 3. The MLP model is constituted by an input layer, 7 fully-connected hidden layers with 700 neurons for each layer, and an output layer. The activation function is ReLU (rectified linear unit) function in the present study. Dropout is introduced to suppress overfitting with a dropout rate of 0.05.

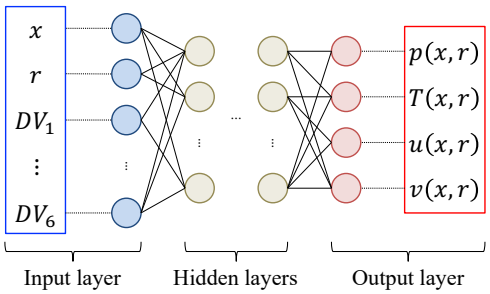

Fig 3. Schematic of flow prediction model using multilayer perceptron

The model is trained with 500 geometries for training and 50 geometries for validation, which are sampled in the design space (Table 1) via Latin hypercube sampling (LHS) [18]. A test dataset with 100 geometries is also generated via LHS. The training is performed by a stochastic gradient-based optimization method Adam [19] with the loss function L:

$$L = \frac{1}{4N} \sum_{m=1}^{N} \sum_{n=1}^{4} \left(y^*_{n,m} - \tilde{y}^*_{n,m} \right) + \lambda \mathbf{w}^{\mathsf{T}} \mathbf{w} \tag{3}$$

where N is the number of data point. y and $\tilde{y}$ are actual and predicted target variables, respectively, and y_1, y_2, y_3, and y_4 represent static pressure, static temperature, and axial and radial velocity components, respectively. The superscript * denotes a variable which is standardized. The 2^{nd} term of the loss function is the regularization term. λ is the coefficient and **w** is the vector composed by weights. The detailed setting of training is summarized in Table 2.

Table 2. Detailed setting of MLP training

Batch size	1024
Number of epoch	250
Learning rate	0.0001
Coefficient of regularization	10^{-5}

2.4.2. Accuracy

Model accuracy has been investigated for 100 test geometries in terms of the flowfields and performance parameters. The prediction accuracy is assessed by using root-mean-squared error RMSE and

coefficient of determination R^2 for both flowfields and performance. The RMSE and R^2 are calculated as follows:

$$\mathrm{RMSE}_y = \sqrt{\frac{1}{N}\sum_{i=1}^{N}(y_i - \tilde{y}_i)^2} \tag{4}$$

$$R_y^2 = 1 - \frac{\sum_{i=1}^{N}(y_i - \tilde{y}_i)^2}{\sum_{i=1}^{N}(y_i - \bar{y})^2} \tag{5}$$

The accuracy of flow prediction is summarized in Table 3.

Table 3. Accuracy of flow prediction

	p^*	T^*	u^*	v^*
RMSE	0.0756	0.1664	0.0969	0.0921
R^2	0.9944	0.9724	0.9906	0.9916

The prediction accuracy of each flowfield is evaluated by absolute and relative errors, E_{abs} and E_{rel}, respectively, as well. The prediction error distributions are visualized for the geometry with the medium total RMSE by comparing with the actual (CFD) data as well as in the form of absolute and relative errors in Fig. 4. It can be seen that the predicted flowfield shows reasonable agreement with the actual data for the entire flowfield, apart from minor increases in prediction errors around shock waves, while the error is marginal.

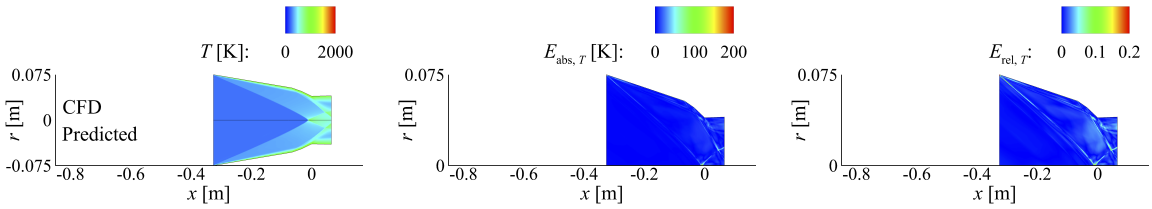

(a) Comparison **(b)** Absolute error **(c)** Relative error

Fig 4. Comparison of static temperature distributions between actual and predicted flowfields and prediction error distributions

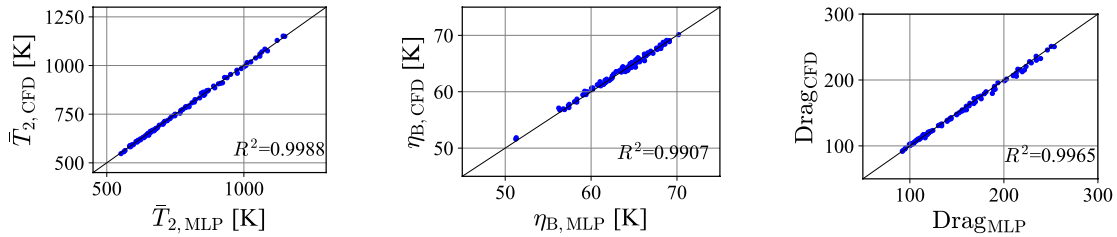

(a) Mean exit temperature **(b)** Compression efficiency **(c)** Drag

Fig 5. Comparison of performance parameters calculated from predicted flowfields and those from actual flowfields for 100 test data

Performance parameters calculated based on predicted flowfields are compared with those calculated from actual flowfields in Fig. 5, along with the coefficients of determination. The blue dots near the

diagonal black line indicate high prediction accuracy. The results signify that the flow prediction model is accurate enough to evaluate intake performance.

The capability of the model for supersonic/hypersonic flow prediction has been demonstrated in the previous study conducted by the authors, and detailed information on the characteristics of the model can be found in Reference [12].

2.5. Computational fluid dynamics

Computational fluid dynamics (CFD) simulations are performed to generate a dataset and to verify prediction results in the present study. A commercial density-based solver ANSYS Fluent 2021 R1 is employed to obtain steady-state flowfields inside scramjet intakes by solving Reynolds-averaged Navier-Stokes (RANS) equations with shear-stress transport (SST) $k-\omega$ turbulence model [20, 21]. The flux is discretized by using AUSM+ (advection upstream splitting method plus) with second-order spatial accuracy and the Green-Gauss cell-based method is used for spatial discretization in the calculations of gradients [22]. The full multigrid acceleration technique and the differentiable limiter are employed for faster and robust convergence. A calorically and ideal gas assumption is employed for the air with a constant specific heat c_p of 1006.43 J/(kg·K) and the gas constant of 287 J/(kg·K). The viscosity is calculated by using Sutherland's law.

The internal flowfields of scramjet intakes are represented by two-dimensional structured meshes which are generated via an open-source mesh generator Gmsh [23]. The computational mesh is composed of 120,000 cells with 301 nodes in the steamwise direction and 401 nodes in the radial direction. The mesh size in the radial direction is diminished toward the intake surface to resolve the turbulent boundary layer (the non-dimensional distance from the nearest wall y^+ is less than 1 on the whole), as shown in Fig. 6. The intake surface is assumed to be isothermal with a constant static temperature of 300 K and the other boundary conditions are summarized in Fig. 6.

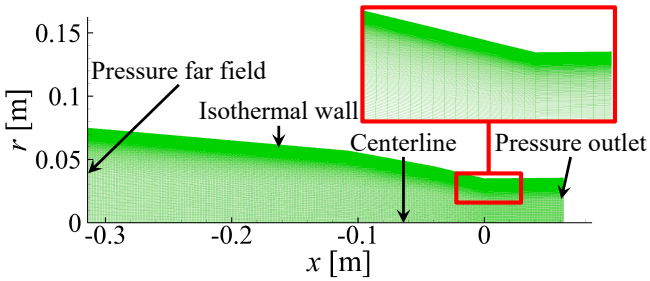

Fig 6. Computational mesh and boundary conditions

The numerical setting and computational mesh are validated in the preceding study [14] and further validation for axisymmetric 3-ramp intakes can be found in References [24, 25].

3. Results

3.1. Validation of MDPAEA

The optimal solution search ability of MDPAEA is investigated for 3 test problems by comparing with NSGA-II. The test problems employed on the preceding study conducted by Deb *et al.* are also employed in the present study. The problem settings are summarized in Table 4. The optimization process is continued until the 45^{th} generation for MDPAEA and the 50^{th} generation for NSGA-II with 200 individuals in the population pool. A training dataset comprising 1000 individuals is used to build models to predict objective/constraint function values, and thus the total number of solution evaluations is the same between MDPAEA and NSGA-II.

The obtained non-dominated solutions are compared between MDPAEA and NSGA-II in Fig. 7. It can be seen that the distributions of non-dominated solutions obtained via MDPAEA contain those obtained via NSGA-II but are more widely spread than them, particularly for CONSTR (Fig. 7 (a)) and TNK (Fig. 7 (c)). This difference in the distributions of non-dominated solutions is attributed to the selection of the initial

Table 4. Test problems used in this study (all objective functions are to be minimized)

Test problem	Variable ranges	Objective functions	Constraint functions
CONSTR	$x_1 \in [0.1, 1]$ $x_2 \in [0, 5]$	$f_1 = x_1$ $f_2 = \frac{1+x_2}{x_1}$	$g_1 = x_2 + 5x_1 \geq 6$ $g_2 = -x_2 + 9x_1 \geq 1$
SRN	$x_1 \in [-20, 20]$ $x_2 \in [-20, 20]$	$f_1 = (x_1 - 2)^2 + (x_2 - 1)^2 + 2$ $f_2 = 9x_1 - (x_2 - 1)^2$	$g_1 = x_1^2 + x_2^2 \leq 225$ $g_2 = x_1 - 3x_2 \leq -10$
TNK	$x_1 \in [0, \pi]$ $x_2 \in [0, \pi]$	$f_1 = x_1$ $f_2 = x_2$	$g_1 = -x_1^2 - x_2^2 + 1 +$ $0.1 \cos\left(16 \arctan\left(\frac{x_1}{x_2}\right)\right) \leq 0$ $g_2 = (x_1 - 0.5)^2 + (x_2 - 0.5)^2 \leq 0.5$

population because the evolutionary procedures of MDPAEA are the same as those of NSGA-II except for the selection of the initial population. Superior individuals have been selected from the training dataset for the initial population of MDPAEA to accelerate solution search, while they have been selected randomly for NSGA-II.

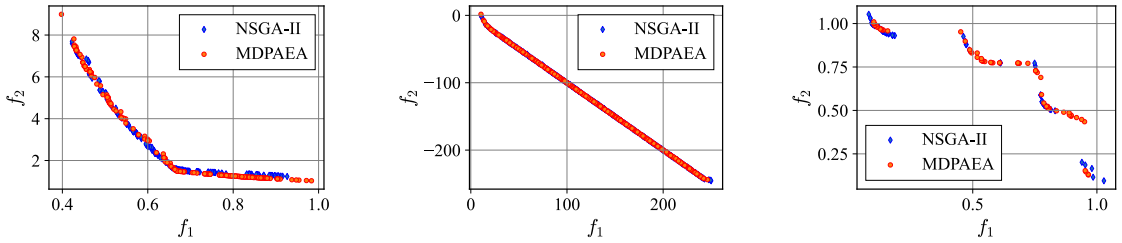

(a) CONSTR **(b)** SRN **(c)** TNK

Fig 7. Comparison of non-dominated solutions obtained via MDPAEA with those obtained via NSGA-II

The number of true function evaluations in the optimization process is also compared between MDPAEA and NSGA-II in Table 5. It has been found that MDPAEA substantially reduces true function evaluations by employing surrogate prediction, in particular in cases of CONSTR and TNK. Compared with these two test problems, SRN requires a considerably larger number of true function evaluations while the number of true function evaluations of MDPAEA is still almost half of that of NSGA-II. This is because the non-dominated solutions of SRN has converged well to the true Pareto front albeit an increase in the number of true function evaluations for validation.

Table 5. Comparison of number of true function evaluations between MDPAEA and NSGA-II

	CONSTR	SRN	TNK
MDPAEA	1251+1000	4691+1000	325+1000
NSGA-II	10000	10000	10000

3.2. Scramjet intake design optimization

3.2.1. Overview and physical insights

Axisymmetric 3-ramp intake design has been optimized in terms of compression efficiency and drag by using MDPAEA. The population of 96 individuals has been evolved to the 30^{th} generation and the model prediction has been employed in the entire optimization process. Thirty-seven non-dominated solutions

have been found from the optimization over 30 generations. The distributions of the resultant solutions are shown in the objective function space and in the form of a parallel coordinate plot in Fig. 8.

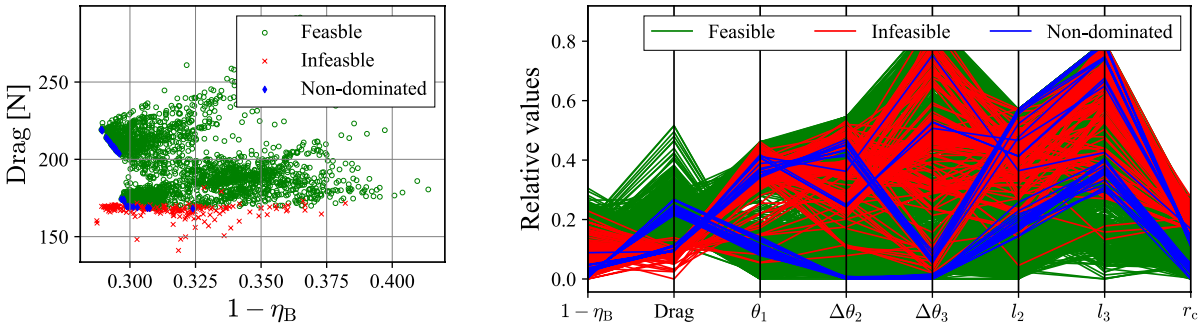

(a) Objective function space

(b) Parallel coordinate plot

Fig 8. Scramjet intake design optimization results

It can be seen in Fig. 8 (a) that the non-dominated solutions can be divided into two groups, *i.e.*, the solutions characterized by high compression efficiency (low compression efficiency loss) and large drag and those that exist near the boundary between feasible and infeasible solutions. Former and latter clusters are named Clusters A and B, respectively, and the solution with the minimum drag and that with the minimum compression efficiency loss are selected from each cluster to scrutinize the characteristics of solutions in each cluster in Fig. 9 (a). It is interesting to note that the compression efficiency of the solution A_2 is close to that of the solution B_1 whereas the drag differs substantially. This indicates that the solutions in each cluster have different characteristics. The geometries of non-dominated solutions are visualized in Fig. 9 (b) and the solutions in Cluster A is longer than those in Cluster B. The flowfields of the selected non-dominated solutions are compared with respect to static temperature distributions in Fig. 10. The large drag of the solutions in Cluster A is caused by a large number of shock reflections that increases pressure drag and longer geometries that increase viscous drag, while high compression efficiency is achieved owing to a large amount of heat transfer across the large intake surface. In contrast, the solutions in Cluster B have shorter geometries, allowing for smaller drag at the cost of reduced compression efficiency.

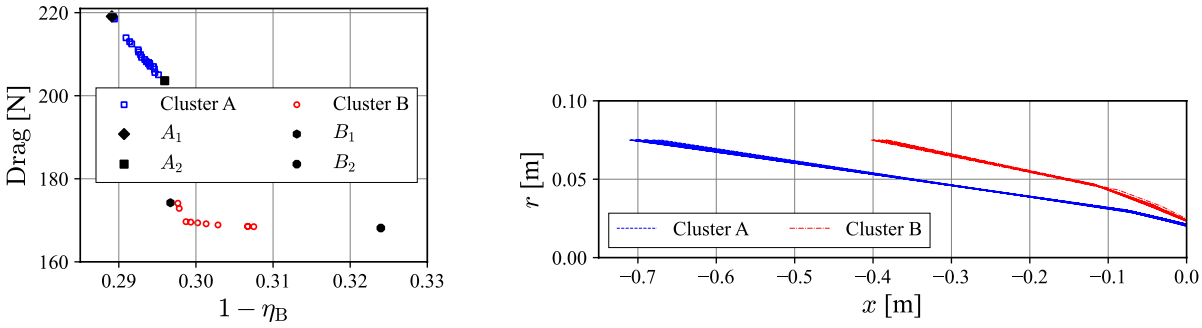

(a) Clusters and selected non-dominated solutions

(b) Geometries of selected non-dominated solutions

Fig 9. Clustering and selection of non-dominated solutions

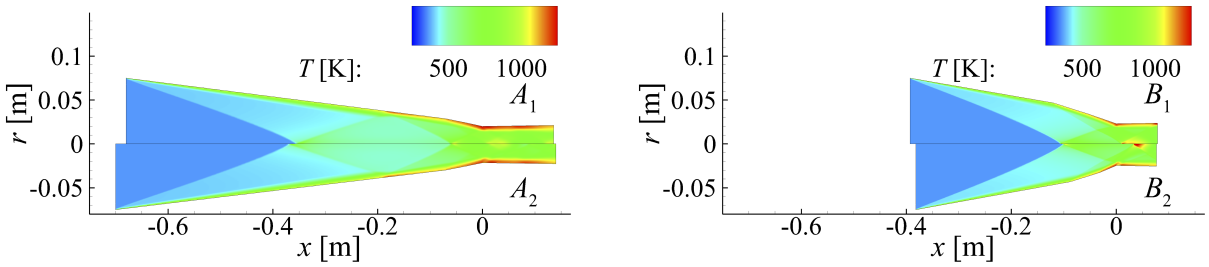

(a) A_1 and A_2 **(b)** B_1 and B_2

Fig 10. Static temperature distributions of selected non-dominated solutions

The optimality of the intake design has been discussed under the calorically perfect gas assumption in the preceding study [14], which allows the optimality of the present non-dominated solutions to be verified theoretically. The distributions of mean exit temperature and heat transfer across intake surface are shown with respect to contraction ratio in Fig. 11. The theory has verified that mean exit temperature should be minimized for the given contaction ratio to minimize both drag and compression efficiency simultaneously and heat transfer causes the trade-off between compression efficiency and drag [14]. As expected from the theory, the resultant non-dominated solutions have the minimum mean exit temperature for given contraction ratio in Fig. 11 (a). The non-dominated solutions in Cluster B have the mean exit temperature around 850 K due to the constraint function and have the possible maximum heat transfer to minimize drag in Fig. 11 (b).

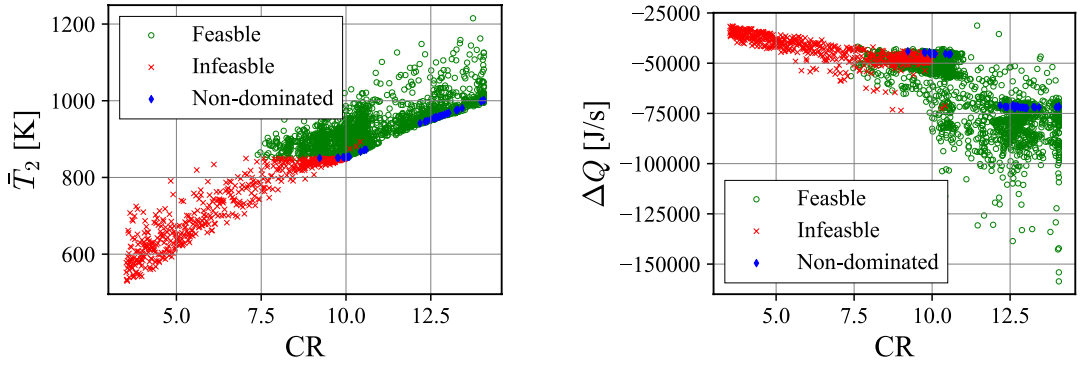

(a) Mean exit temperature **(b)** Heat transfer

Fig 11. Variations of static temperature and heat transfer with respect to contraction ratio

All individuals evaluated by CFD or prediction have been employed in the analysis for Fig. 11. Fast flowfield prediction allows for the generation of an informative physics-based database, without which it would be difficult to gain physical insight into performance parameters other than objective/constraint functions at a low computational cost. The availability of predicted flowfields and the prediction model thus enables various post analyses.

3.2.2. Performance of MDPAEA

The performance of MDPAEA is assessed from the viewpoint of computational cost and prediction accuracy. Figure 12 compares the number of true function evaluations (CFD simulations) between MDPAEA and NSGA-II. Similarly to the results of the test problems in Table 5, the number of true function evaluations is also reduced to less than 50 % of NSGA-II for the intake design optimizaton by replacing

them with model prediction. This indicates that MDPAEA can allow for a larger population size compared to NSGA-II at the same computational cost. Another main factor of the computational cost is the training of the prediction model. In the present study, a multilayer perceptron neural network is employed and requires relatively large computational cost for training. The computational time for training and re-training with 200 additional training data is summarized in Table 6. While the present model requires a larger computational cost to provide prediction of multi-dimensional output, the fidelity of the predictive model is higher than those of general surrogate models which predict a scalar value, being capable of predicting flowfields at a high fidelity that is comparable to that of the true function evaluation. Furthermore, MDPAEA can save the total computational cost in comparison with NSGA-II. It can thus be said that MDPAEA can reduce the computational cost while maintaining the fidelity of the solution search, whereas general surrogate-assisted/based EA can reduce the computational cost at the penalty of reduced fidelity.

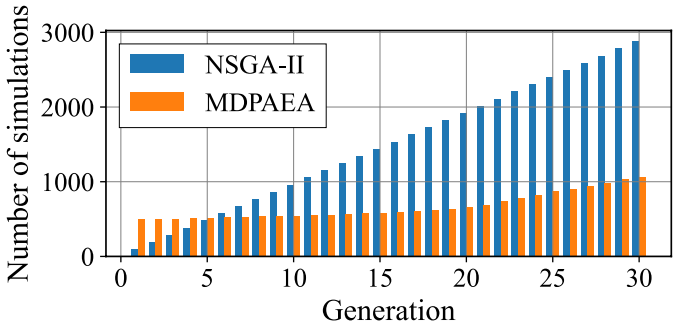

Fig 12. Comparison of numbers of CFD simulations (true function evaluations)

Table 6. Comparison of computation time for training among models

	Original model	Retrained with 200 additional training data
1 epoch [sec]	317.2	444.1
Total [h]	22.03	3.08

The accuracy of the prediction model used in the optimization is investigated for two test datasets, *i.e.*, (1) the dataset via LHS which represents the entire design space and (2) the test dataset obtained in the optimization process which includes the individuals near the Pareto optimal front comprising the non-dominated solutions. The prediction accuracy for those datasets is compared among the original model and those retrained every 10 generations in Fig. 13. It has been found that the total RMSE for the test data via LHS is similar among the 4 models (Fig. 13 (a)) and the total RMSE for the data obtained in the optimization process decreases as the number of generation hence the number of retraining increases (Fig. 13 (b)). This indicates that the prediction accuracy for the individuals near the Pareto optimal front is improved by the retraining process, whereas that for the entire design space is not affected, as seen in Figs. 13 (b) and (a), respectively. Since the prediction is accurate enough for the entire design space and much more accurate for the individuals in the vicinity of the Pareto optimal front, the model can be applied to the post analysis as well as other studies such as optimization and parametric studies. This conduces to efficient knowledge discovery for the subject of optimization.

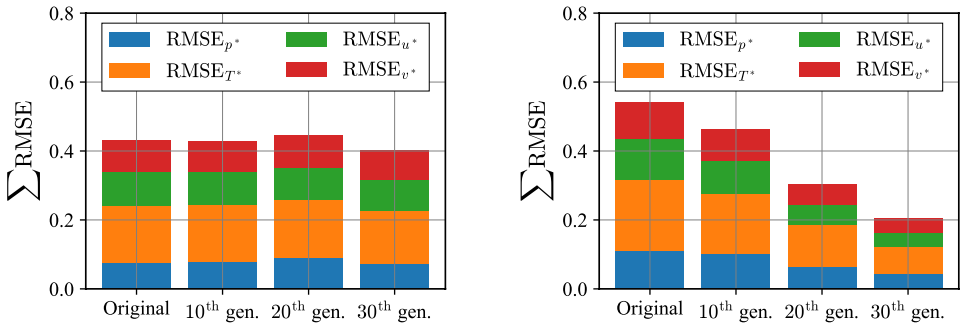

(a) Test data via LHS **(b)** Test data obtained in optimization process

Fig 13. Variations of model accuracy through retraining

4. Conclusions

The present study has proposed an evolutionary algorithm assisted by multi-dimensional predictive modeling via deep learning to realize a high-fidelity and low-cost design optimization of scramjet intakes. The algorithm employs the prediction of flowfields inside scramjet intakes using a multilayer perceptron. The proposed algorithm is applied to several mathematical optimization test problems for validation and an optimization study of axisymmetric 3-ramp scramjet intake design. The utility and applicability are then examined by scrutinizing the optimization results.

The algorithm of the proposed methodology is based on a non-dominated sorting evolutionary algorithm NSGA-II and the performance is therefore assessed in comparison with NSGA-II for several test problems. The proposed approach has substantially reduced the total number of true function evaluations, albeit the cost required to prepare datasets for multi-dimensional predictive modeling. It is interesting to note that the proposed methodology tends to yield a widespread Pareto optimal front than that obtained via NSGA-II. The difference is attributed to the difference in the selection of the initial population.

An optimization study of axisymmetric 3-ramp intakes has then been conducted using the multi-dimensional prediction assisted evolutionary algorithm. The flow prediction model has been retrained every 10 generations in the optimization process using the CFD data which are obtained to verify the provisional non-dominated solutions. This improves the prediction accuracy for the individuals around the Pareto optimal front without deteriorating the global prediction accuracy. The post analysis has been conducted not only for the non-dominated solutions but also the other solutions by scrutinizing the physics-based dataset generated via flow prediction and CFD. The large number of predicted flowfields has offered useful insights into not only objective/constraint functions but also other performance parameters, demonstrating the reasonable ability of design exploration.

While the present study focuses on the development of the multi-dimensional prediction assisted evolutionary algorithm to reduce the number of true function evaluations, another advantage of the proposed algorithm is the reusability of the flow prediction model. Since the prediction accuracy of the model is improved in the optimization process, the model can be employed in different studies such as design optimization with different objective/constraint functions or different algorithms and sensitivity analysis. The ability of flexible post analysis is a key to elucidating the rationales of excellent design. Further effort will be dedicated to enhancing the utility of the multi-dimensional prediction assisted evolutionary algorithms, aiming to realize high-fidelity but low-cost design exploration and knowledge discovery for fluid engineering.

Acknowledgments

The authors acknowledge the support provided by the Japan Society for the Promotion of Science through the KAKENHI Grant number 17K20144 and the Grant-in-Aid for JSPS Fellows Grant Number 22J20613 as well as the Japan Science and Technology Agency through the JST SPRING Grant Number JPMJSP2136.

References

[1] Curran, E.T.: Scramjet Engines: The First Forty Years. J. Propuls. Power. 17, 1138–1148 (2001) https://doi.org/10.2514/2.5875.

[2] Urzay, J.: Supersonic Combustion in Air-Breathing Propulsion Systems for Hypersonic Flight. Annu. Rev. Fluid Mech. 50. 593–627 (2018) https://doi.org/10.1146/annurev-fluid-122316-045217.

[3] Deb, K.: Multi-Objective Optimization using Evolutionary Algorithms. Wiley, New York (2009)

[4] Oyama, A., Nonomura, T., Fujii, K.: Data Mining of Pareto-Optimal Transonic Airfoil Shapes Using Proper Orthogonal Decomposition. J. Aircr. 47, 1756–1762 (2010) https://doi.org/10.2514/1.C000264.

[5] Chiba, K., Obayashi, S.: Knowledge Discovery for Flyback-Booster Aerodynamic Wing Design Using Data mMining. J. Spacecr. Rockets. 45, 975–987 (2008) https://doi.org/10.2514/1.28511.

[6] Fujio, C., Ogawa, H.: Physical insights into multi-point global optimum design of scramjet intakes for ascent flight. Acta Astronaut. 194, 59–75 (2022) https://doi.org/10.1016/j.actaastro.2022.01.036

[7] Forrester, A.I.J., Keane, A.J.: Recent advances in surrogate-based optimization. Prog. Aerosp. Sci. 45, 50–79 (2009) https://doi.org/10.1016/j.paerosci.2008.11.001.

[8] Brunton, S.L., Noack, B.R., Koumoutsakos, P.: Machine Learning for Fluid Mechanics. Annu. Rev. Fluid Mech. 52, 477–508 (2020) https://doi.org/10.1146/annurev-fluid-010719-060214.

[9] Bui-Thanh, T., Damodaran, M., Willcox, K.: Aerodynamic Data Reconstruction and Inverse Design Using Proper Orthogonal Decomposition, AIAA J. 42, 1505–1516 (2004) https://doi.org/10.2514/1.2159.

[10] Schmid, P.J.: Dynamic mode decomposition of numerical and experimental data. J. Fluid Mech. 656, 5–28 (2010) https://doi.org/10.1017/S0022112010001217.

[11] Sekar, V., Jiang, Q., Shu, C., Khoo, B.C.: Fast flow field prediction over airfoils using deep learning approach. Phys. Fluids. 31 (2019). https://doi.org/10.1063/1.5094943.

[12] Fujio, C., Ogawa, H.: Deep-learning prediction and uncertainty quantification for scramjet intake flowfields. Aerosp. Sci. Technol. preprint (2022)

[13] Boyce, R. R., Tirtey, S. C., Brown, L., Creagh, M., Ogawa, H.: SCRAMSPACE : Scramjet-Based Access-to-Space Systems. 17th AIAA International Space Planes and Hypersonic Systems and Technologies Conference, San Francisco, CA (2011)

[14] Fujio, C., Ogawa, H.: Theoretical Characterization and Multi-Objective Optimization of Scramjet Intake Performance. J. Propuls. Power, under review (2022)

[15] Ogawa, H., Boyce, R.R.: Physical Insight into Scramjet Inlet Behavior via Multi-Objective Design Optimization. AIAA J. 50, 1773–1783 (2012) https://doi.org/10.2514/1.j051644.

[16] Deb, K., Pratap, A., Agarwal, S., Meyarivan, T.: A Fast and Elitist Multiobjective Genetic Algorithm: NSGA-II. IEEE Trans. Evol. Comput. 6 (2002) 182–197.

[17] Abadi, M., Barham, P., Chen, J., Chen, Z., Davis, A., Dean, J., Devin, M., Ghemawat, S., Irving, G., Isard, M., Kudlur, M., Levenberg, J., Monga, R., Moore, S., Murray, D. G., Steiner, B., Tucker, P., Vasudevan, V., Warden, P., Wicke, M., Yu, Y., Zheng, X.: TensorFlow: A System for Large-Scale

Machine Learning. in: proceeding of 12th USENIX Symp. Oper. Syst. Des. Implement. (OSDI 16), USENIX Association, pp. 265–283. Savannah, GA (2016)

[18] Stein, M.: Large sample properties of simulations using latin hypercube sampling. Technometrics. 29, 143–151 (1987) https://doi.org/10.1080/00401706.1987.10488205.

[19] Kingma, D.P., Ba, J.L.: Adam: A method for stochastic optimization, in: proceeding of 3rd Int. Conf. Learn. Represent. pp.1–15. San Diego, CA (2015)

[20] ANSYS FLUENT User's Guide. ANSYS Inc., Canonsburg, PA (2021)

[21] Menter, F.R.: Two-Equation Eddy-Viscosity Turbulence Models for Engineering Applications. AIAA J. 32 (1994). https://doi.org/10.2514/3.12149.

[22] Liou, M.S.: A sequel to AUSM: AUSM+. J. Comput. Phys. 129, 364–382 (1996) https://doi.org/10.1006/jcph.1996.0256.

[23] Geuzaine, C.: Gmsh : A 3-D finite element mesh generator with built-in pre- and post-processing facilities, Int. J. Numer. Methods Eng. 79, 1309–1331 (2009) https://doi.org/10.1002/nme.

[24] Brahmachary, S., Fujio, C., Ogawa, H.: Multi-point design optimization of a high-performance intake for scramjet-powered ascent flight. Aerosp. Sci. Technol. 107, 106362 (2020) https://doi.org/10.1016/j.ast.2020.106362.

[25] Fujio, C., Brahmachary, S., Ogawa, H.: Numerical investigation of axisymmetric intake flowfield and performance for scramjet-powered ascent flight. Aerosp. Sci. Technol. 111, 106531 (2021) https://doi.org/10.1016/j.ast.2021.106531.